Compressive Residual Strains in Mineral Nanoparticles as a Possible Origin of Enhanced Crack Resistance in Human Tooth Dentin

Jean-Baptiste Forien,[†] Claudia Fleck,[‡] Peter Cloetens,[§] Georg Duda,[†] Peter Fratzl,[⊥] Emil Zolotoyabko,[¶] Paul Zaslansky[†]

[†]Julius Wolff Institute, Charité – Universitätsmedizin, 13353 Berlin, Germany
[‡]Materials Engineering, Berlin Institute of Technology, 10623 Berlin, Germany
[§]European Synchrotron Radiation Facility, 38043 Grenoble, France
[⊥]Department of Biomaterials, Max-Planck-Institute of Colloids and Interfaces, 14424 Potsdam, Germany
[¶]Department of Materials Science and Engineering, Technion – Israel Institute of Technology, 32000 Haifa, Israel

Supporting Information

Sample preparation

Human teeth were obtained from anonymous, routine dental-care patients, collected following the directives of the institutional ethics committee of the Charité - Universitätsmedizin Berlin School of Dental Medicine. Eight teeth, extracted for orthodontic or periodontal reasons, were stored refrigerated in a chloramine 0.5% solution. Dentin was harvested from the roots of molars and premolars, after removal of the thin layer of cementum covering the roots, identified by the very different microstructure lacking tubules. Preference was given to root dentin since it has much less PTD and is less mineralized than crown dentin;[1] furthermore, collagen in root dentin has well-defined preferred orientations.[2] Consequently, crystallographic textures of the collagen-associated apatite are easier to detect in X-ray diffraction patterns in the roots than in crown dentin.[3] From each tooth, several slices were cut using a slow speed water-cooled diamond saw (Isomet Buehler Ltd. Lake Bluff, Illinois, USA). Concomitantly, each slice was subjected to grinding and polishing, using emery sheets (water used as a coolant), to reach uniform thicknesses of 250 ~ 400 μm for in situ annealing diffraction experiments, and about 200 μm for diffraction nanotomography

experiments. Bar-shaped samples for diffraction mapping, about 0.4×0.4×20 mm^3 in size, were cut by longitudinal sectioning, more or less following the long axis of the micron-sized dental tubules (Figure S1). In samples of this thickness, tubules run a parallel course with little or no change in their trajectories, as verified by optical microscopy, as is known for both molar and premolar human teeth.[4]

Six bar-shaped specimens (cut from three different teeth) were measured in both dry and hydrated states, whereas four specimens underwent heat treatment in an oven at 220 °C with a 50 min holding time as shown in the temperature ramping of the oven in Figure S2. All samples were air-dried for 24 h under ambient (~35% relative humidity at ~23 °C) conditions. Three larger samples from other teeth, 0.25×5×25 mm^3 in size, prepared for the in situ annealing experiments, had larger dimensions in order to fit the sample holder of the beamline diffractometer. To track and correct for any thermal deformation-induced sample drifts, half of the wider X-ray mapped surface was gold-coated using a sputter coater (Cressington Scientific Instruments Ltd, Hertfordshire, England). Sputtering at 40 mA for 240 s resulted in approximately 120 nm thick gold layer, just visible to the naked eye.

Diffraction nanotomography

Dentin slices, 200 μm thick, were used to prepare splinters for diffraction nanotomography experiments at the ID22-NI beamline[5] of the European Synchrotron Radiation Facility (ESRF, Grenoble, France). Datasets were collected using a 17 keV X-rays focused down to a 120x120 nm^2 beam size, produced by a multilayer-coated Kirkpatrick-Baez (KB) mirror system. Each sample was positioned on an electro-mechanical goniometer stage located 130 mm upstream of a Fast Readout Low Noise (FReLoN) camera equipped with the de-magnifying taper optics (52 μm pixel size). Diffraction patterns were acquired using 0.2 s exposure times, and were performed by scanning across horizontal planes of the sample, mounted on its edge, such that the tubules followed a

vertical course (see schematics in Figure 2 in the main text). Three hundred diffraction patterns (with 1 μm lateral increments) were collected on lines extending across the sample width, and after each line-scan, the sample was rotated (ω) by 3º through a total of 60 angular projections spanning 180° around the sample axis.

Phase contrast enhanced nanotomography to visualize tubules in dentin

Using the same ID22-NI setup described above[5], the dentin splinters were scanned by applying projected zoom tomography with an effective pixel size of ~175 nm. Owing to the partial coherence of X-ray at this beamline, we were able to carry out phase contrast-enhanced nanotomography of the micron-sized tubules. Specifically, several tomographic scans were performed employing different propagation distances (each with 1999 projections, spanning 360 deg around the sample axis, 0.1 s exposures). Due to the large refractive index differences at the dentin sample boundaries and at each interfaces between the lower density tubule voids and the surrounding higher density of PTD and ITD, backprojection reconstruction of the data contains sever streaks and strong intensity fluctuations near feature edges. To better visualize the tubules within the sample geometry, phase filtering using the Paganin approach was employed by the aid of the ESRF PyHST 2 code[6] and taking a delta/beta ratio as 1000 to minimize low frequency artefacts. Two-dimensional reconstructed phase-retrieved slices, using two different propagation distances (5 mm apart) are shown in Figure S3. Note that these slices were obtained from the same sample region as the diffraction tomography slices in Figure 2.

Diffraction mapping of dentin texture and in situ annealing experiments

Measurements were carried out at the my-Spot beamline of BESSY II (Berlin, Germany). To increase X-ray flux and shorten exposure times, a multilayered monochromator was used, tilted to produce a beam energy of 15 keV.[7] Diffraction patterns were collected using a MarMosaic 225 detector (Mar USA, Evanston, USA), positioned 204.7 mm downstream of the sample. Detector

orientation, rotation, and sample-detector distance were calibrated using diffraction from a powdered quartz standard.

Diffraction patterns were collected by raster-scanning (along x,z, axes see Figure 3 in main text) the bar-shaped samples, mounted all in parallel, by moving the samples normal to their long axes and gradually shifting the sample holder upwards, through a 75 μm diameter beam (see schematics in Figure 3a). Thus, each sample was measured in multiple adjacent neighboring points, moved both laterally and along the tooth-root axis so as to prevent radiation damage by accidentally irradiating any sampling point more than once. Exposure times of 2 s were used, and 15-20 non-overlapping diffraction patterns were collected for each sample. After scanning the air-dried samples, the sample holder was encased in a thin polyimide (Kapton) foil to create a small hydrated chamber. A second set of diffraction patterns was collected following rehydration by immersion in water, while maintaining the samples still on the sample holder in the beam line setup. The radiation dose for each diffraction pattern was estimated according to Deymier et. al.[8] Based on these estimations, we found the X-ray dose to be 34 ± 4 kGy that corresponds to the lower limit of damaging radiation, observed in dentin in such experiments.

A beam size of 50x50 μm² was used for the in situ annealing experiments. Samples were mounted in a Linkam heating chamber (THMS600) and raster scanned (x,z), with horizontal and vertical steps of 200 and 500 μm, respectively, ensuring no overlap between neighboring diffraction patterns due to radiation damage concerns as mentioned above. About fifty diffraction patterns were recorded per sample, with a 5 s exposure time each. Data was collected at room temperature and also following heating at 125 °C, further heating to 250 °C, holding for 0.5 h at 250 °C and, finally, upon cooling to room temperature. The samples were heated at the rate of 4 °C/min, and the temperature was maintained constant during diffraction pattern acquisition. In these measurements,

due to a different configuration of the beamline optics, flux density was lower and radiation damage did not exceed 15 kGy.

Data analysis

All diffraction data were analyzed using the XRDUA analysis kit.[9] For the diffraction tomography experiments, calibration parameters were refined using the (002), (310) and (222) Debye rings of the dentin sample. The (002) peak intensity of dentin (appearing between 11.3° to 12.8° on the 2θ-scale) was azimuthally integrated over 36 regions of the Debye ring, each spanning 10°. Integrated intensities of the diffraction patterns were converted into sinograms and then tomographically reconstructed. A maximum likelihood expectation maximization iterative tomographic reconstruction (mlem) algorithm was used with 10 iterations.[9]

To improve the precision of our analysis in the quantitative diffraction experiments, the apatite *c*-axis lattice parameter was determined by tracking the (002) peak position in several regions of the Debye ring. In each diffraction pattern, the maxima and minima of the (002) diffraction intensities were identified, corresponding to the subtle "on-axis" and "off-axis" collagen-fiber texture, respectively (see Figure 3c). We performed azimuthal intensity integrations over an angular range of 7° at the center of these on/off axis regions, with each arc divided into sub-sectors of 1° that were later averaged. All plots were fitted using a pseudo-Voigt model function. Opposite positions of the rings, corresponding to the same texture orientations, were averaged for both “on-axis” and the “off-axis” peak positions. By determining the peak positions in the neighboring and opposite sectors, it was possible to derive mean and standard deviations of the peak positions, based on several different non-identical crystal families that reside in dentin at approximately the same orientation and presumably have the same strain state.

For the in situ annealing experiments, the “on-axis” peak positions were determined, as described above, and then further processed. The (111) diffraction intensity of the sputtered gold

was azimuthally integrated over its Debye ring and the extracted (111) gold *d*-spacing was used as a reference, to correct for heat-induced sample-to-detector distance shifts. To obtain correct apatite *c-axis* lattice constants, we used the relationship:

$$\Delta d_{ap} = \frac{\cos^2 \theta_{ap} \cos 2\theta_{ap}}{\cos^2 \theta_g \cos 2\theta_g} \cdot \frac{\Delta d_g}{d_g} \cdot d_{ap} \qquad \text{(S1)}$$

where *d* represents the measured *d*-spacings in apatite (ap) and gold (g) respectively, Δd_g is the difference between the measured and tabulated gold *d*-spacings at any given measurement temperature, and Δd_{ap} is the difference between the observed and corrected *c*-axis lattice parameter of apatite at each temperature; diffraction angles for the (002) apatite reflection and (111) gold reflection are marked as θ_{ap} and θ_g, respectively.

Collagen diffraction-pattern analysis

Analysis of the small-angle X-ray scattering signal from in situ annealed dentin samples (Figure S4) allowed us to compare the collagen diffraction patterns obtained at room temperature, at elevated temperatures (125 °C, 250 °C) and after 1 h annealing at 250 °C. This analysis showed that although the collagen signal becomes very weak already at 125 °C, the Debye rings are still visible and can be used to extract the lateral collagen spacing. The latter reveals substantial heating-induced shrinkage, as previously reported.[10] This structural change occurs on an orthogonal orientation with respect to the "on-axis" (002) diffraction intensity peak of the mineral (Figure 3 and S4). This provides additional evidence that the strongly compressed mineral is oriented along the collagen fibrils.

References

(1) Weber, D. F. *J. Morphol.* **1968**, *126* (4), 435–445.
(2) Wang, R. Z.; Weiner, S. *J. Biomech.* **1998**, *31* (2), 135–141.
(3) Zaslansky, P.; Maerten, A.; Fratzl, P. *Bioinspired Biomim. Nanobiomaterials* **2013**, *2* (4), 194–202.
(4) Zaslansky, P.; Zabler, S.; Fratzl, P. *Dent. Mater.* **2010**, *26* (1), e1–e10.
(5) Martínez-Criado, G.; Tucoulou, R.; Cloetens, P.; Bleuet, P.; Bohic, S.; Cauzid, J.; Kieffer, I.; Kosior, E.; Labouré, S.; Petitgirard, S.; Rack, A.; Sans, J. A.; Segura-Ruiz, J.; Suhonen, H.; Susini, J.; Villanova, J. *J. Synchrotron Radiat.* **2012**, *19* (1), 10–18.
(6) Mirone, A.; Brun, E.; Gouillart, E.; Tafforeau, P.; Kieffer, J. *Nucl. Instrum. Methods Phys. Res. B.* **2014**, *324*, 41–48.
(7) Paris, O.; Li, C.; Siegel, S.; Weseloh, G.; Emmerling, F.; Riesemeier, H.; Erko, A.; Fratzl, P. *J. Appl. Crystallogr.* **2006**, *40* (s1), s466–s470.
(8) Deymier-Black, A. C.; Almer, J. D.; Stock, S. R.; Dunand, D. C. *J. Mech. Behav. Biomed. Mater.* **2012**, *5* (1), 71–81
(9) De Nolf, W.; Vanmeert, F.; Janssens, K. *J. Appl. Crystallogr.* **2014**, *47* (3), 1107–1117.
(10) Hayashi, M.; Koychev, E. V.; Okamura, K.; Sugeta, A.; Hongo, C.; Okuyama, K.; Ebisu, S. *J. Dent. Res.* **2008**, *87* (8), 762–766.
(11) Zabler, S.; Riesemeier, H.; Fratzl, P.; Zaslansky, P. *Opt. Express* **2006**, *14* (19), 8584–8597.
(12) Zabler, S.; Cloetens, P.; Zaslansky, P. *Opt. Lett.* **2007**, *32* (20), 2987–2989.

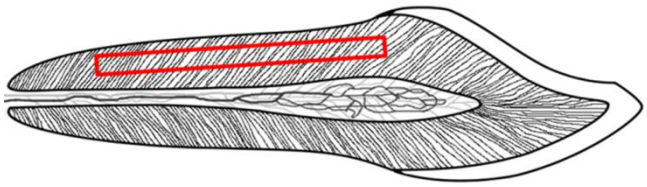

Figure S1. *Schematic illustration of one of the teeth used (human canine) with indication of the source of the harvested samples. The red rectangle shows the approximate origin of the final bar-shaped specimen within the root.*

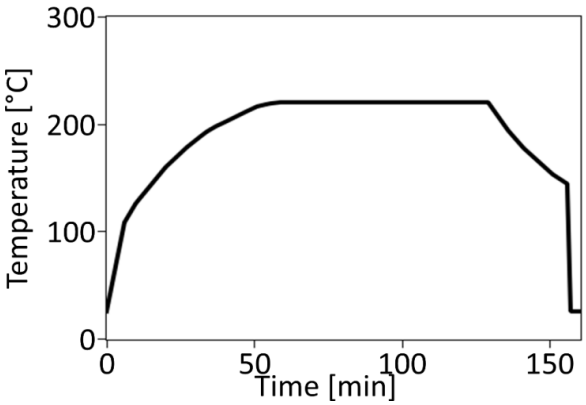

Figure S2. *Typical annealing (heating to 220 °C in air) temperature evolution for heat-treated dentin samples.*

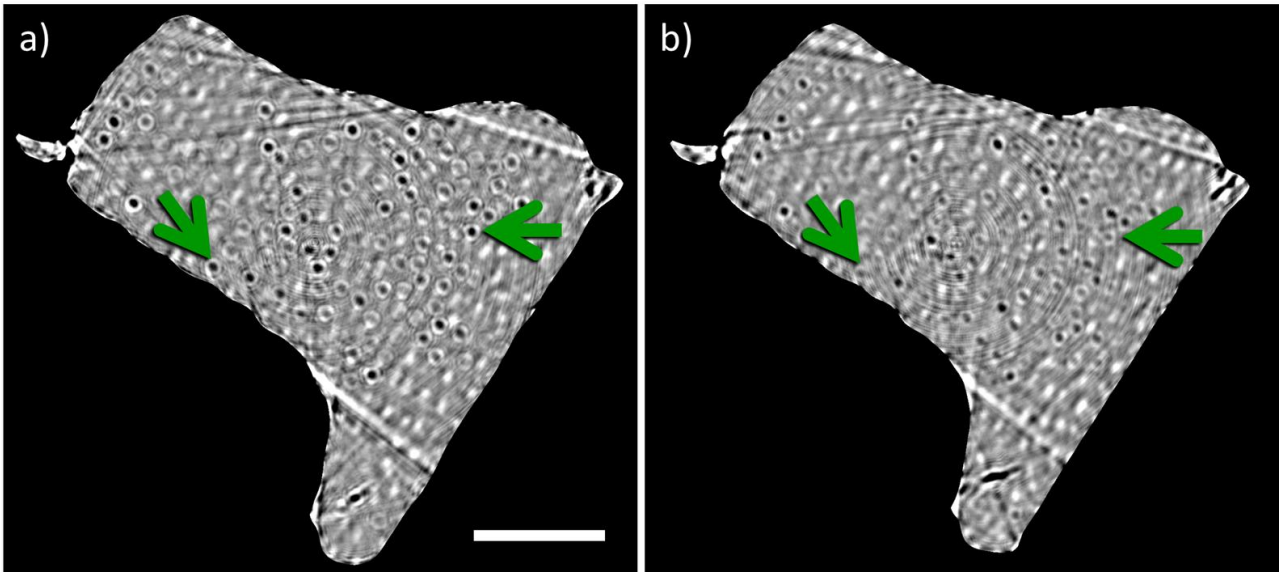

Figure S3. *Reconstructed slices of phase contrast-enhanced nanotomography scans acquired from the same sample used for the diffraction tomography slices shown in Figure 2 using a propagation distance of (a) 403.5 mm and (b) 398.5 mm. Experimental details are given in the relevant SI section above. Note the much higher spatial resolution of this data (~175 nm) as compared with the diffraction tomography (1 μm) shown in Figure 2. The patent, low density voids of the tubules can be seen as either bright spots or as dark spots surrounded by bright rings, the contrast varying as a function of detector distance (compare arrows pointing to the same tubule at different distances). As previously shown by Zabler et al.,*[11,12] *the visibility of the tubules strongly depends on the tubule and PTD diameters/thicknesses, as well as the physical parameters of the beamline (resolution, distance, coherence and energy used). Scale Bar: 50 μm*

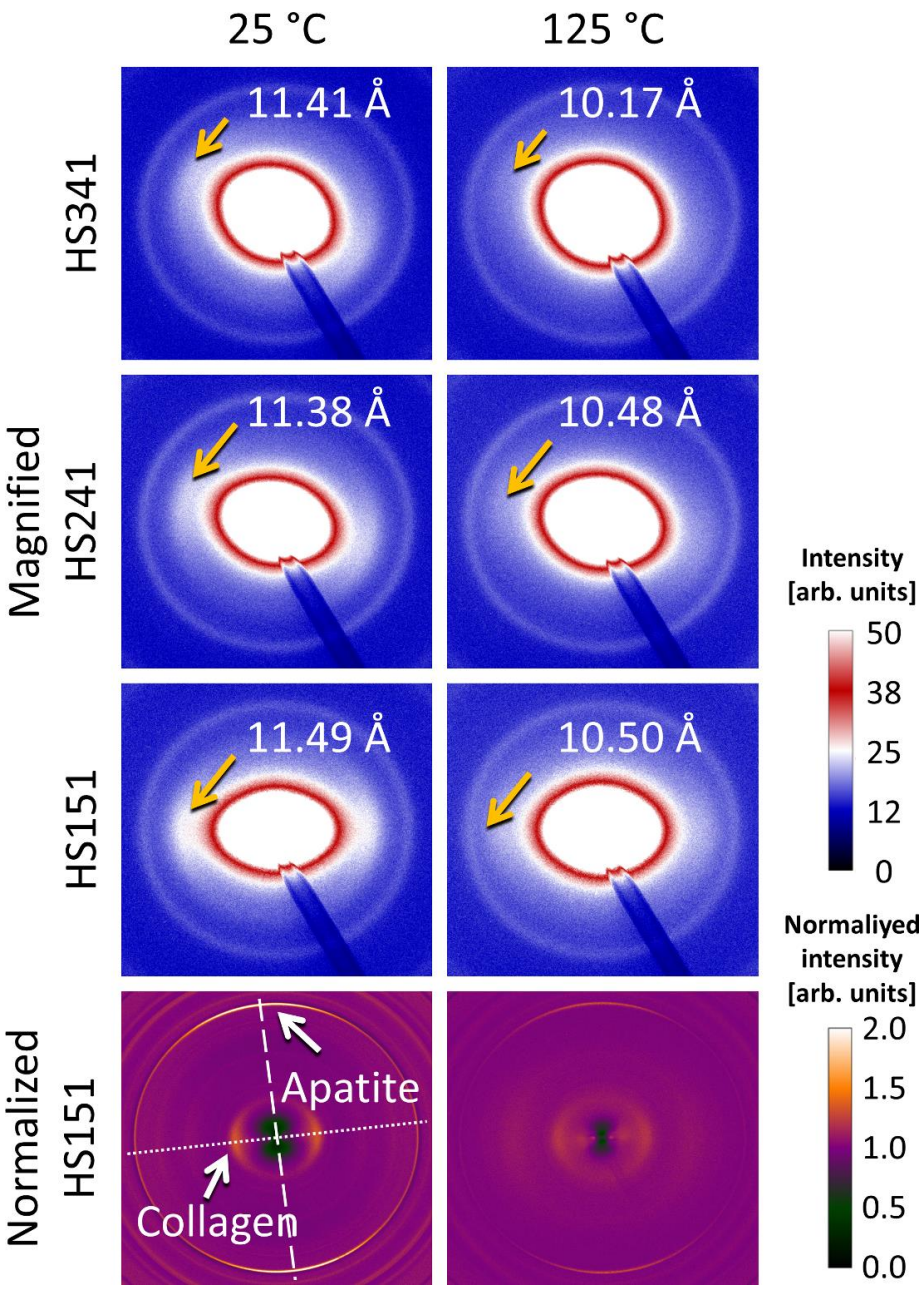

Figure S4. *Magnified zones of small angle collagen diffraction patterns: The data show the lateral packing of collagen fibrils, in three different samples (identified as HS341, HS241, and HS151) during the in situ annealing experiment. The X-ray meridian collagen peak positions reveal clear changes in the lateral packing of the fibrils in the collagen fibers, when comparing diffraction patterns collected at room temperature (25 °C, left-hand column) and those collected after heating to 125 °C (right-hand column). Similar to previous reports*[8] *we observe a shrinkage of the collagen lateral spacing from 11.43 ± 0.06 Å to 10.38 ± 0.19 Å. Bottom panel: visual proof fot the orthogonal spatial relationship between the orientation of the collagen lateral spacing (small angle signal) and the apatite 002 diffraction peak arcs (wide angle signal). Images were obtained by normalizing the diffraction patterns using an empty beam. This presentation highlights the mutual co-alignment of collagen fibrils and the majority of the mineral crystallite c-axes. This provides corroboratory evidence that our in situ measurements of collagen lateral contraction and mineral strain are from the mineralized collagen fibers in the ITD dentin matrix.*

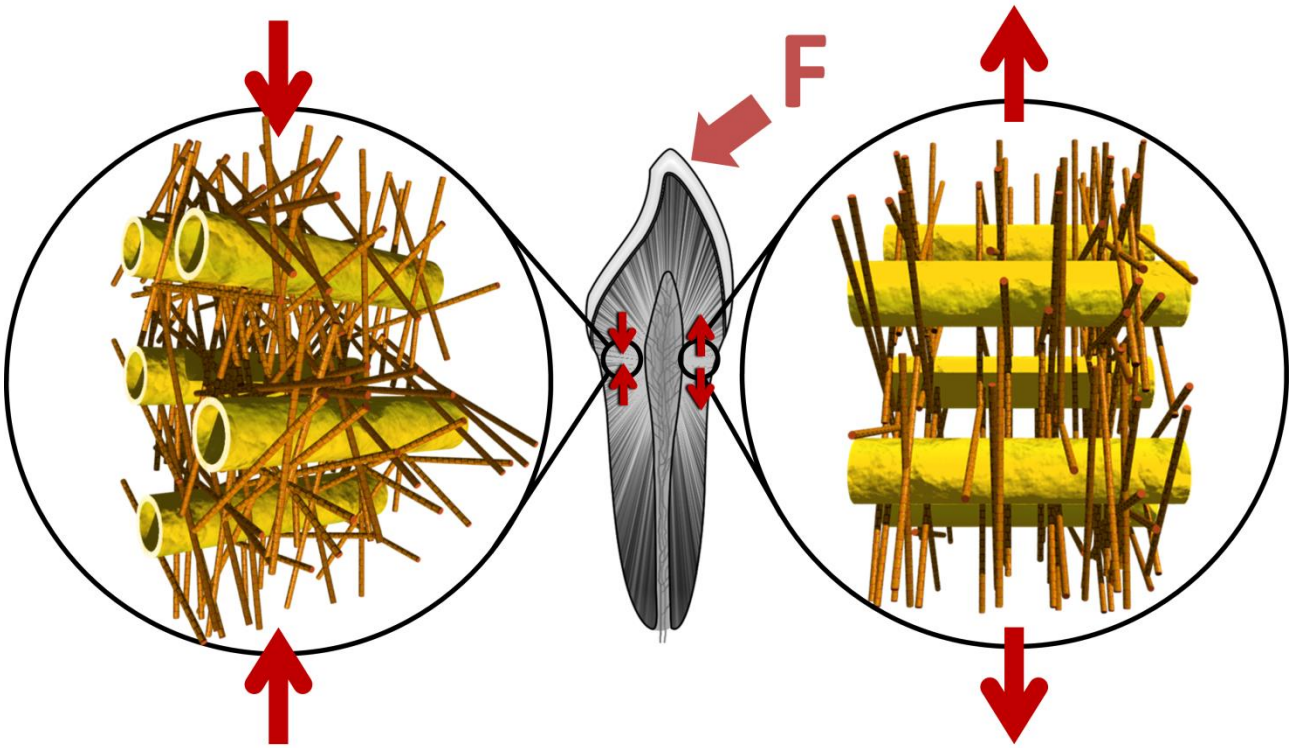

Figure S5. *Schematic representation of typical forces and stresses acting on teeth. The tubules and collagen fibers are shown schematically in the magnification circles on both sides of the tooth. During mastication, teeth transmit forces (F, red arrows) that break-down nutrition products. Consequently, stress is transmitted into dentin through the outer stiff (highly mineralized) enamel cap layer. This leads to the emergence of bending moments such that in various regions in dentin, tensile stresses arise across tubule trajectories, along the collagen fibril layers. We propose that the residual compressive stresses that we identified along the mineralized collagen fibrils serve to counteract such tensile stresses in dentin, protecting the microstructure from cracking. Furthermore, as compressed mineral is firmly attached to the collagen, the collagen fibrils are in tension since the net force applied to the entire unloaded structure is zero. Such tension offers additional protection against fibril buckling under compression, further reducing the danger of bending the fibers, which would lead to fracture when the bulk of dentin is loaded in compression during mastication.*